J. Fluid Mech. (2010), *vol.* 662, *pp.* 475–492. © Cambridge University Press 2010
doi:10.1017/S0022112010003320

Convection–dissipation instability in the horizontal plane Couette flow of a highly viscous fluid

A. BARLETTA[1]† AND D. A. NIELD[2]

[1]Dipartimento di Ingegneria Energetica, Nucleare e del Controllo Ambientale (DIENCA), Università di Bologna, Via dei Colli 16, I–40136 Bologna, Italy

[2]Department of Engineering Science, University of Auckland, Private Bag 92019, Auckland 1142, New Zealand

(Received 5 February 2010; revised 18 June 2010; accepted 18 June 2010; first published online 28 September 2010)

The linear stability of the plane Couette flow against thermoconvective rolls is studied. The case of a flow without a boundary-imposed temperature gradient is investigated. The non-uniform, possibly unstable, basic temperature distribution is caused by the effect of the internal viscous heating. Asymmetric thermal boundary conditions are considered: the bottom boundary is adiabatic, while the top boundary is isothermal. The focus is on a fluid with a large, mathematically infinite, Prandtl number, although the two-dimensional transverse roll instability is discussed also for a finite Prandtl number. The transition to the instability is described through the governing parameter $Ge\,Pe^2$, where Ge is the Gebhart number and Pe is the Péclet number. The response of the basic Couette flow to arbitrarily oriented oblique rolls is tested, so that a complete set of disturbance modes is taken into account. It is shown that the Couette flow is more unstable to longitudinal rolls than to any other oblique roll mode.

Key words: absolute/convective instability, buoyancy-driven instability, general fluid mechanics

1. Introduction

It is well known that the plane Couette flow has no linear hydrodynamic instability. This fact is widely discussed in the literature as, for instance, in Drazin & Reid (2004). The first rigorous proof of the linear stability of plane Couette flow is attributed to Romanov (1973). This author studied the evolution of the normal modes through the analysis of the Orr–Sommerfeld equation, showing that these modes are always damped, for every value of the Reynolds number.

Although the hydrodynamic instability is absent in the plane Couette flow, an instability of thermal origin may arise. In fact, the hydrodynamic equations, i.e. the local mass and momentum balance equations, may develop a coupling with the local energy balance equation. The coupling term in the local momentum balance equation, may be either the viscous force through a temperature-dependent viscosity of the fluid, or the gravitational body force through a thermal buoyancy effect. The origin of the

† Email address for correspondence: antonio.barletta@unibo.it

temperature gradient that drives this energy–momentum coupling can be either the prescribed thermal boundary conditions or the viscous dissipation effect.

The role of the viscous dissipation as a possible source of instability was explored in the pioneering work of Joseph (1965). This author pointed out that the plane Couette flow, with wall temperatures a prescribed constant, may be linearly unstable due to the viscous dissipation effect and to a temperature-dependent viscosity of the fluid. In Joseph (1965), no buoyancy effect was considered, and the linear stability analysis was performed with respect to the inviscid (infinite Reynolds number) Orr–Sommerfeld equation. Sukanek, Goldstein & Laurence (1973) further developed the study initiated by Joseph (1965), with the same boundary conditions and maintaining the assumption of negligible buoyancy effects. The analysis of Sukanek *et al.* (1973) refers to finite Reynolds numbers and leads to the numerical evaluation of the critical conditions for the onset of instability for a special viscosity–temperature relationship, i.e. an exponential law. These authors show that, when either the viscous dissipation is switched off or the viscosity is a constant, the Couette flow is stable, which is the result reported in Drazin & Reid (2004) and proved by Romanov (1973). More precise numerical results based on a fourth-order Runge–Kutta method were obtained by Ho, Denn & Anshus (1977), with respect to the same assumptions and boundary conditions defined in Sukanek *et al.* (1973). The effects of different types of temperature-dependent viscosity models, the Nahme law and the Arrhenius law, on the thermal instability of plane Couette flow have been explored by Yueh & Weng (1996). Johns & Narayanan (1997) and Subrahmaniam, Johns & Narayanan (2002) investigated other aspects of the problem studied by Joseph (1965). Quite recently, the analysis of the viscous dissipation instability of the plane Couette flow has been extended to non-Newtonian fluids by Nouar & Frigaard (2009). We point out the common characteristics of all these papers originated from Joseph's analysis:

(*a*) they consider the destabilizing role of the interplay between the viscous dissipation and the temperature-dependent viscosity;

(*b*) they neglect the buoyancy force;

(*c*) they assume that the same uniform temperature is prescribed on the two plane boundary walls.

The above literature survey is intended just to allow us to distinguish our own study from the previous works and is not meant to be definitive. Much more could be said about the investigations initiated with Joseph (1965). In this connection, a referee has pointed out to us that the study by Joseph (1965) was predicated on disturbances with 'zero' wavenumber, and made it seem that the wall stress was a control variable (which it is not).

A closely related subject is the buoyancy-induced instability of the plane Couette flow due to a uniform vertical temperature gradient. This subject has been studied by Ingersoll (1966) and, more recently, by Fujimura & Kelly (1988) in the more general case of the Poiseuille–Couette flow. These papers refer to a fluid layer bounded by rigid isothermal walls with an externally imposed temperature difference. Ingersoll (1966) and Fujimura & Kelly (1988) evaluated the critical Rayleigh number for the onset of the thermoconvective instability, as a function of the Reynolds number associated with the basic Couette flow. These authors show that the critical Rayleigh number is an increasing function of the Reynolds number and it tends to the well-known critical value of the Rayleigh–Bénard instability, 1707.67, when the Reynolds number tends to zero.

The aim of this paper is to investigate the linear stability of the plane Couette flow induced by the interplay between the viscous dissipation and the buoyancy

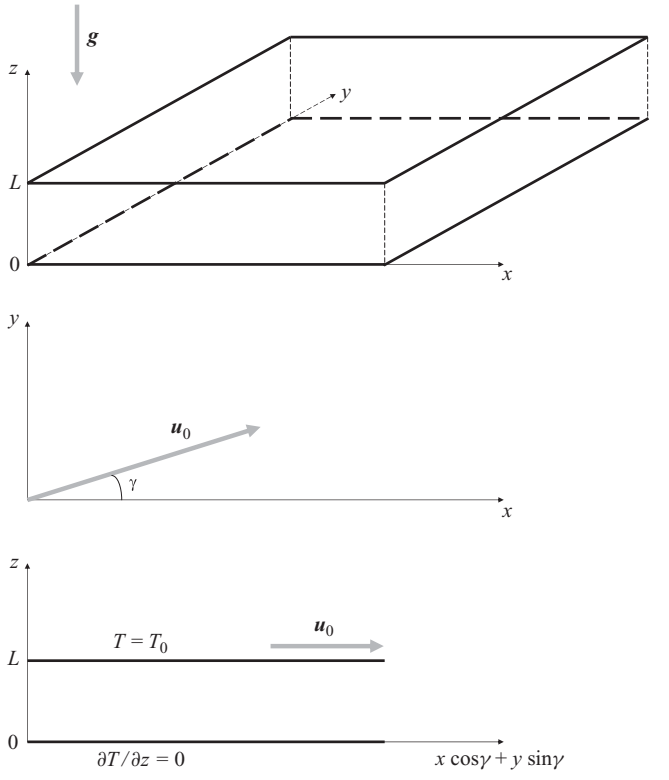

FIGURE 1. A sketch of the fluid layer and of the coordinate system.

force, on assuming a constant viscosity. In other words, we are interested in the thermoconvective instability activated by the viscous dissipation. The non-uniform character of the basic temperature distribution will be assumed to be entirely due to the frictional heating, and not to an external temperature difference imposed through the boundary conditions. In fact, we will consider the case of an adiabatic bottom wall at rest and an isothermal top moving wall. We will refer to a highly viscous fluid such that the Prandtl number is much larger than unity. This assumption allows us to consider a complete set of oblique roll disturbances, with any possible orientation with respect to the basic flow. Finally, the reliability of the highly viscous fluid approximation is assessed by comparison with the case of a finite Prandtl number, for transverse modes. We emphasize that this paper contains, to the best of our knowledge, the first analysis of the linear instability of the plane Couette flow due to the viscous dissipation and the buoyancy force, in the absence of an imposed temperature difference at the boundary walls.

2. Couette flow with viscous dissipation

Let us consider plane Couette flow between the two horizontal boundaries $z = 0$ and $z = L$, where $(x_i) = (x, y, z)$ are the Cartesian coordinates of the reference frame defined in figure 1. We denote by: $\boldsymbol{u} = (u_i)$ the velocity field; T the temperature field; p the pressure field; ρ_0 the fluid density at the reference temperature T_0; β the thermal expansion coefficient; $\boldsymbol{g} = (g_i)$ the gravitational acceleration; ν the kinematic viscosity; $\mu = \nu\,\rho_0$ the dynamic viscosity; c the heat capacity per unit mass;

k the thermal conductivity; $\alpha = k/(\rho_0 c)$ the thermal diffusivity. Finally, we denote by $\mathfrak{D}_{ij}$ the strain tensor:

$$\mathfrak{D}_{ij} = \frac{1}{2}\left(\frac{\partial u_i}{\partial x_j} + \frac{\partial u_j}{\partial x_i}\right). \tag{2.1}$$

According to the Oberbeck–Boussinesq approximation, the governing equations are

$$\frac{\partial u_j}{\partial x_j} = 0, \tag{2.2}$$

$$\frac{\partial u_i}{\partial t} + u_j \frac{\partial u_i}{\partial x_j} = -\frac{1}{\rho_0}\frac{\partial p}{\partial x_i} - (T - T_0)\beta g_i + \nu \nabla^2 u_i, \tag{2.3}$$

$$\rho_0 c\left(\frac{\partial T}{\partial t} + u_j \frac{\partial T}{\partial x_j}\right) = k\nabla^2 T + 2\mu\, \mathfrak{D}_{ij}\, \mathfrak{D}_{ij}, \tag{2.4}$$

where sums over repeated indices are implied. The boundary conditions are

$$\left.\begin{aligned} &z = 0 : \boldsymbol{u} = (0, 0, 0), \quad \frac{\partial T}{\partial z} = 0, \\ &z = L : \boldsymbol{u} = (u_0 \cos\gamma, u_0 \sin\gamma, 0), \quad T = T_0. \end{aligned}\right\} \tag{2.5}$$

The thermal boundary conditions correspond to a vanishingly small conductance of the bottom wall and an infinite conductance of the top moving wall. As illustrated in figure 1, the top wall moves at a constant velocity $\boldsymbol{u}_0$, with $u_0 = |\boldsymbol{u}_0|$, along the direction of the horizontal unit vector $(\cos\gamma, \sin\gamma, 0)$, where γ is any angle such that $0 \leqslant \gamma \leqslant \pi/2$.

2.1. *Dimensionless variables*

Let us consider the following transformation of the dependent and independent variables:

$$\left.\begin{aligned} &\frac{x_i}{L} \to x_i, \quad \frac{t\alpha}{L^2} \to t, \quad \frac{u_i L}{\alpha} \to u_i, \quad \frac{(T - T_0)kL^2}{\mu\alpha^2} \to T, \\ &\frac{pL^2}{\mu\alpha} \to p, \quad \frac{L^2 \mathfrak{D}_{ij}}{\alpha} \to \mathfrak{D}_{ij}. \end{aligned}\right\} \tag{2.6}$$

Then, (2.2)–(2.5) are written in a dimensionless form,

$$\frac{\partial u_j}{\partial x_j} = 0, \tag{2.7}$$

$$\frac{1}{Pr}\left(\frac{\partial u_i}{\partial t} + u_j \frac{\partial u_i}{\partial x_j}\right) = -\frac{\partial p}{\partial x_i} + GeT\delta_{i3} + \nabla^2 u_i, \tag{2.8}$$

$$\frac{\partial T}{\partial t} + u_j \frac{\partial T}{\partial x_j} = \nabla^2 T + 2\,\mathfrak{D}_{ij}\,\mathfrak{D}_{ij}, \tag{2.9}$$

$$\left.\begin{aligned} &z = 0 : \boldsymbol{u} = (0, 0, 0), \quad \frac{\partial T}{\partial z} = 0, \\ &z = 1 : \boldsymbol{u} = (Pe \cos\gamma, Pe \sin\gamma, 0), \quad T = 0. \end{aligned}\right\} \tag{2.10}$$

A basic time-independent solution of (2.7)–(2.9) subject to (2.10) is sought such that:

(i) the velocity field $\boldsymbol{u} = (u, v, w)$ is parallel and oriented horizontally along the direction of the top wall velocity;

(ii) the fields T and p depend only on z.

One has

$$\left.\begin{aligned} u_B = Pez\,\cos\gamma, \quad v_B = Pe\;z\;\sin\gamma, \quad w_B = 0, \\ T_B = \frac{Pe^2}{2}\left(1-z^2\right), \quad p_B = \frac{GePe^2}{2}\left(z-\frac{z^3}{3}\right), \end{aligned}\right\} \tag{2.11}$$

where the subscript B stands for 'basic flow'.

In (2.7)–(2.10), δ_{ij} is Kronecker's delta and the dimensionless parameters

$$Pr = \frac{\nu}{\alpha}, \quad Ge = \frac{\beta g L}{c}, \quad Pe = \frac{u_0 L}{\alpha}, \tag{2.12}$$

are the Prandtl number, the Gebhart number and the Péclet number, respectively.

We believe that our choice of scaling for the non-dimensionalization is the appropriate one for the problem in hand. However, to aid comparison with previous studies which have been expressed in terms of a Reynolds number, we mention that if alternatively we used a velocity scale u_0 instead of α/L (so that the ratio of the new scale to the old scale is Pe), and consistent with this a time scale L/u_0 instead of L^2/α, and define

$$\tilde{u} = u/Pe, \quad \tilde{t} = Pe\,t, \quad \tilde{p} = p/(Pe\;Re), \quad \tilde{T} = T/Pe^2, \quad \tilde{\mathfrak{D}}_{ij} = \mathfrak{D}_{ij}/Pe, \tag{2.13}$$

where the Reynolds number Re is given by $Re = Pe/Pr$, then (2.8) and (2.9) take the forms

$$\frac{\partial \tilde{u}_i}{\partial \tilde{t}} + \tilde{u}_j \frac{\partial \tilde{u}_i}{\partial x_j} = -\frac{\partial \tilde{p}}{\partial x_i} + GePr\;\tilde{T}\,\delta_{i3} + \frac{1}{Re}\nabla^2 \tilde{u}_i, \tag{2.14}$$

$$Pe\left(\frac{\partial \tilde{T}}{\partial \tilde{t}} + \tilde{u}_j\,\frac{\partial \tilde{T}}{\partial x_j}\right) = \nabla^2 \tilde{T} + 2\,\tilde{\mathfrak{D}}_{ij}\,\tilde{\mathfrak{D}}_{ij}. \tag{2.15}$$

3. Linear disturbances

Let us consider small perturbations, of order ε, of the basic Couette flow (2.11):

$$(u, v, w) = (u_B, v_B, w_B) + (U, V, W)\,\varepsilon, \quad p = p_B + P\varepsilon, \quad T = T_B + \theta\varepsilon. \tag{3.1}$$

By substituting (3.1) into (2.7)–(2.9) subject to (2.10) and neglecting terms of order ε^2, one obtains

$$\frac{\partial U}{\partial x} + \frac{\partial V}{\partial y} + \frac{\partial W}{\partial z} = 0, \tag{3.2}$$

$$\frac{1}{Pr}\left(\frac{\partial U}{\partial t} + Pez\,\cos\gamma\,\frac{\partial U}{\partial x} + Pez\,\sin\gamma\frac{\partial U}{\partial y} + PeW\,\cos\gamma\right) = -\frac{\partial P}{\partial x} + \nabla^2 U, \tag{3.3}$$

$$\frac{1}{Pr}\left(\frac{\partial V}{\partial t} + Pez\,\cos\gamma\,\frac{\partial V}{\partial x} + Pez\,\sin\gamma\frac{\partial V}{\partial y} + PeW\,\sin\gamma\right) = -\frac{\partial P}{\partial y} + \nabla^2 V, \tag{3.4}$$

$$\frac{1}{Pr}\left(\frac{\partial W}{\partial t} + Pez\,\cos\gamma\,\frac{\partial W}{\partial x} + Pez\,\sin\gamma\frac{\partial W}{\partial y}\right) = -\frac{\partial P}{\partial z} + Ge\theta + \nabla^2 W, \tag{3.5}$$

$$\begin{aligned} \frac{\partial \theta}{\partial t} + Pez\left(\cos\gamma\frac{\partial \theta}{\partial x} + \sin\gamma\frac{\partial \theta}{\partial y} - PeW\right) &= \nabla^2\theta \\ &\quad + 2\,Pe\left[\cos\gamma\left(\frac{\partial U}{\partial z} + \frac{\partial W}{\partial x}\right) + \sin\gamma\left(\frac{\partial V}{\partial z} + \frac{\partial W}{\partial y}\right)\right], \end{aligned} \tag{3.6}$$

$$\left.\begin{aligned} z = 0 &: (U, V, W) = (0, 0, 0), \quad \frac{\partial \theta}{\partial z} = 0, \\ z = 1 &: (U, V, W) = (0, 0, 0), \quad \theta = 0. \end{aligned}\right\} \tag{3.7}$$

3.1. *A highly viscous fluid: large-Pr approximation*

Let us now assume that the fluid is highly viscous (kinematic viscosity much greater than the thermal diffusivity) so that $Pr \to \infty$. This implies that the inertial terms in the local momentum balance equation can be neglected (creeping flow). The approximation consists in assuming a very large Prandtl number, together with a very small Reynolds number, so that the Péclet number is a finite quantity. Then, the disturbance equations (3.2)–(3.7) can be simplified to

$$\frac{\partial U}{\partial x} + \frac{\partial V}{\partial y} + \frac{\partial W}{\partial z} = 0, \tag{3.8}$$

$$\nabla^2 U - \frac{\partial P}{\partial x} = 0, \tag{3.9}$$

$$\nabla^2 V - \frac{\partial P}{\partial y} = 0, \tag{3.10}$$

$$\nabla^2 W - \frac{\partial P}{\partial z} + Ge\,\theta = 0, \tag{3.11}$$

$$\frac{\partial \theta}{\partial t} + Pez\left(\cos\gamma\,\frac{\partial \theta}{\partial x} + \sin\gamma\,\frac{\partial \theta}{\partial y} - PeW\right) = \nabla^2\theta + 2\,Pe\left[\cos\gamma\left(\frac{\partial U}{\partial z} + \frac{\partial W}{\partial x}\right) + \sin\gamma\left(\frac{\partial V}{\partial z} + \frac{\partial W}{\partial y}\right)\right], \tag{3.12}$$

$$\left.\begin{aligned} z = 0 &: (U, V, W) = (0, 0, 0), \quad \frac{\partial \theta}{\partial z} = 0, \\ z = 1 &: (U, V, W) = (0, 0, 0), \quad \theta = 0. \end{aligned}\right\} \tag{3.13}$$

According to the normal mode decomposition of the disturbance, one can consider a two-dimensional roll arbitrarily oriented, i.e. oblique, with respect to the basic velocity field by assuming

$$U = U(x, z, t), \quad V = 0, \quad W = W(x, z, t), \quad \theta = \theta(x, z, t), \quad P = P(x, z, t). \tag{3.14}$$

Equation (3.14) defines arbitrary two-dimensional disturbances in the xz-plane. Then, (3.10) is identically satisfied, while (3.8), (3.9) and (3.11)–(3.13) yield

$$\frac{\partial U}{\partial x} + \frac{\partial W}{\partial z} = 0, \tag{3.15}$$

$$\nabla^2\left(\frac{\partial U}{\partial z} - \frac{\partial W}{\partial x}\right) - Ge\,\frac{\partial \theta}{\partial x} = 0, \tag{3.16}$$

$$\frac{\partial \theta}{\partial t} + Pez\left(\cos\gamma\,\frac{\partial \theta}{\partial x} - PeW\right) = \nabla^2\theta + 2\,Pe\,\cos\gamma\left(\frac{\partial U}{\partial z} + \frac{\partial W}{\partial x}\right), \tag{3.17}$$

$$\left.\begin{aligned} z = 0 &: (U, W) = (0, 0), \quad \frac{\partial \theta}{\partial z} = 0, \\ z = 1 &: (U, W) = (0, 0), \quad \theta = 0, \end{aligned}\right\} \tag{3.18}$$

where (3.16) has been obtained from (3.9) and (3.11) by differentiating (3.9) with respect to z, differentiating (3.11) with respect to x and then subtracting the latter resulting equation from the former one.

Let us introduce the streamfunction ψ such that

$$U = Ge\frac{\partial \psi}{\partial z}, \quad W = -Ge\frac{\partial \psi}{\partial x}. \tag{3.19}$$

Thus, (3.15) is identically satisfied, while (3.16)–(3.18) can be rewritten as

$$\nabla^4 \psi - \frac{\partial \theta}{\partial x} = 0, \tag{3.20}$$

$$\frac{\partial \theta}{\partial t} + Pez\left(\cos\gamma \frac{\partial \theta}{\partial x} + GePe\ \frac{\partial \psi}{\partial x}\right) = \nabla^2\theta + 2\,GePe\,\cos\gamma\left(\frac{\partial^2 \psi}{\partial z^2} - \frac{\partial^2 \psi}{\partial x^2}\right), \tag{3.21}$$

$$\left.\begin{aligned} z = 0 : \psi = 0, \quad \frac{\partial \psi}{\partial z} = 0, \quad \frac{\partial \theta}{\partial z} = 0, \\ z = 1 : \psi = 0, \quad \frac{\partial \psi}{\partial z} = 0, \quad \theta = 0, \end{aligned}\right\} \tag{3.22}$$

where $\nabla^4 = \nabla^2\nabla^2$. Let us consider the plane wave solutions of (3.20)–(3.22) defined by

$$\psi(x, z, t) = \mathrm{Re}\left[\mathrm{i}\, f(z)\, \mathrm{e}^{\lambda t}\, \mathrm{e}^{\mathrm{i}(ax - \omega t)}\right], \quad \theta(x, z, t) = \mathrm{Re}\left[h(z)\, \mathrm{e}^{\lambda t}\, \mathrm{e}^{\mathrm{i}(ax - \omega t)}\right], \tag{3.23}$$

where Re[ ] denotes the real part of a complex function. In (3.23), we have split the disturbance growth rate into its real and imaginary parts, so that both λ and ω are real. The parameter λ is positive for unstable rolls, negative for stable rolls and zero at marginal stability. In the following, we will focus on the marginal stability condition so that we will set $\lambda = 0$. Then, on substituting (3.23) in (3.20)–(3.22), one obtains

$$f'''' - 2a^2 f'' + a^4 f - ah = 0, \tag{3.24}$$

$$h'' - [a^2 + \mathrm{i}(a\,Pe\,z\,\cos\gamma - \omega)]h + 2\mathrm{i}\,\cos\gamma\,\frac{\Lambda}{Pe}\,f'' + \frac{\Lambda}{Pe}\,a(Pe\,z + 2\,\mathrm{i}\,a\,\cos\gamma)f = 0, \tag{3.25}$$

$$\left.\begin{aligned} z = 0 : f = 0, \quad f' = 0, \quad h' = 0, \\ z = 1 : f = 0, \quad f' = 0, \quad h = 0, \end{aligned}\right\} \tag{3.26}$$

where

$$\Lambda = GePe^2. \tag{3.27}$$

and the primes denote derivatives with respect to z.

The use of the parameter Λ instead of the Gebhart number is a convenient choice, as will become evident from the discussion of the results below. In fact, at the onset of the instability, the most physically significant cases are such that the Gebhart number is very small, while the parameter Λ has a value independent of Ge and Pe. In particular, a finite value of Λ yields the critical condition for the onset of longitudinal rolls. We mention that the same dimensionless parameter, $GePe^2$, has been introduced in Barletta, Celli & Rees (2009) and in Nield & Barletta (2010). These papers investigate the onset of the thermoconvective instability in a fluid saturated porous medium governed by Darcy's law, with a basic horizontal throughflow and a non-negligible viscous dissipation.

4. Numerical solution

The pair of ordinary differential equations (3.24) and (3.25) are homogeneous with homogeneous boundary conditions, (3.26). This feature leads to the formulation of an eigenvalue problem, where (γ, Pe, a) are the input parameters. Then, the pair (ω, Λ) is determined as an eigenvalue corresponding to the eigenfunction pair (f, h). We mention that the eigenvalue problem is not self-adjoint, as $f(z)$ and $h(z)$ are complex valued functions.

A numerical solution of (3.24)–(3.26) can be sought by using the fourth-order Runge–Kutta technique. An initial-value problem formulation can be based on (3.24) and (3.25) and on the initial conditions

$$\left.\begin{array}{l} f(0)=0, \quad f'(0)=0, \quad f''(0)=\xi_1+\mathrm{i}\xi_2, \quad f'''(0)=\eta_1+\mathrm{i}\eta_2, \\ h(0)=1, \quad h'(0)=0. \end{array}\right\} \tag{4.1}$$

In fact, (4.1) is based on (3.26), as well as on the possibility of fixing arbitrarily the overall scale of the eigenfunction pair (f, h) through the condition $h(0)=1$. The yet unknown real parameters $(\xi_1, \xi_2, \eta_1, \eta_2)$, together with the eigenvalue pair (ω, Λ), can be obtained by imposing, through a shooting method, the six real constraint equations:

$$\left.\begin{array}{lll} \mathrm{Re}[f(1)]=0, & \mathrm{Re}[f'(1)]=0, & \mathrm{Re}[h(1)]=0, \\ \mathrm{Im}[f(1)]=0, & \mathrm{Im}[f'(1)]=0, & \mathrm{Im}[h(1)]=0, \end{array}\right\} \tag{4.2}$$

implied by (3.26), where Im[ ] denotes the imaginary part of a complex function.

The numerical integration of (3.24)–(3.25) under the initial conditions (4.1) can be carried out within the Mathematica 7.0 (© Wolfram, Inc.) environment. More precisely, we can use function `NDSolve`, with the assignment `Method` → "`ExplicitRungeKutta`". In Mathematica 7.0, the built-in Runge–Kutta method includes an adaptive step-size control so that the step size, δz, need not be assigned. Finally, the shooting method can be implemented through the constraints (4.2) by means of the function `FindRoot`. The optimal order of the Runge–Kutta method is automatically established by the code.

The numerical solutions obtained by the above procedure can be collected so that, for every given value of Pe, one has a parametric function $\Lambda(a)$. The minimum of this function corresponds to the critical conditions for the onset of the convective instability, namely $a=a_{cr}$ and $\Lambda=\Lambda_{cr}$.

4.1. *Oblique, longitudinal and transverse rolls*

The eigenvalue problem is solved numerically for an arbitrary inclination angle γ between the basic flow direction and the x-axis, where $0 \leqslant \gamma \leqslant \pi/2$. We will call *transverse rolls* the disturbances such that $\gamma=0$ and *longitudinal rolls* the disturbances such that $\gamma=\pi/2$.

4.2. *Longitudinal rolls*

Let us consider longitudinal rolls ($\gamma=\pi/2$) with $\omega=0$, then (3.24)–(3.26) yield

$$f''''-2a^2f''+a^4f-ah=0, \tag{4.3}$$

$$h''-a^2h+\Lambda azf=0, \tag{4.4}$$

$$\left.\begin{array}{lll} z=0: f=0, & f'=0, & h'=0, \\ z=1: f=0, & f'=0, & h=0. \end{array}\right\} \tag{4.5}$$

Equations (4.3)–(4.5) form a self-adjoint eigenvalue problem, so that $f(z)$ and $h(z)$ are real-valued functions.

A roughly approximate analytical solution of (4.3)–(4.5) may be sought by employing a first-order Galerkin method of weighted residuals (see, for instance, Finlayson & Scriven 1966). We approximate $f(z)$ and $h(z)$ through a pair of trial functions, $\varphi_1(z)$, $\varphi_2(z)$, satisfying the boundary conditions (4.5),

$$f(z) \cong A\,\varphi_1(z), \quad h(z) \cong \varphi_2(z), \tag{4.6}$$

where

$$\varphi_1(z) = (1-z)^2 z^2, \quad \varphi_2(z) = 1 - z^2, \tag{4.7}$$

and we have invoked the scale fixing condition $h(0) = 1$. For a given a, the coefficient A in (4.6) will be determined together with Λ by substitution in (4.3) and (4.4). More precisely, from (4.3) and (4.4), one obtains the pair of residuals

$$E_1(z) = A\varphi_1''''(z) - 2a^2 A\,\varphi_1''(z) + a^4 A\,\varphi_1(z) - a\varphi_2(z), \tag{4.8}$$

$$E_1(z) = \varphi_2''(z) - a^2\,\varphi_2(z) + \Lambda a z A \varphi_1(z). \tag{4.9}$$

By prescribing the orthogonality between each residual and the corresponding trial function, namely

$$\int_0^1 E_1(z)\,\varphi_1(z)\,\mathrm{d}z = 0, \quad \int_0^1 E_2(z)\,\varphi_2(z)\,\mathrm{d}z = 0, \tag{4.10}$$

one obtains

$$A \cong \frac{15a}{a^4 + 24a^2 + 504}, \quad \Lambda \cong \frac{224(2a^2+5)(a^4+24a^2+504)}{135a^2}. \tag{4.11}$$

We now find the minimum of function $\Lambda(a)$ defined by (4.11), thus determining a rough estimate of the critical conditions for the onset of instability,

$$a_{cr} \cong 2.4, \quad \Lambda_{cr} \cong 3.2 \times 10^3. \tag{4.12}$$

By using the Runge–Kutta numerical solution and the shooting method with (4.3)–(4.5), we obtain extremely accurate critical values (a_{cr}, Λ_{cr}), namely

$$a_{cr} = 2.62929, \quad \Lambda_{cr} = 2772.27. \tag{4.13}$$

Equation (4.12) may be considered as an approximation of the exact result, (4.13), with a 9 % error for a_{cr} and a 15 % error for Λ_{cr}.

We mention that the numerical values displayed in (4.13) are not new in the literature on convective instability. In particular, they have been found by Roberts (1967) in the linear stability analysis of a fluid layer with a uniform internal heat generation and bounded by a pair of plane parallel rigid walls at rest. Roberts' analysis has been further developed by Tveitereid & Palm (1976), Hamabata & Takashima (1983) and Takashima (1991). In these papers, the basic solution is one of vanishing velocity, and not Couette flow as in the present study. Furthermore, 2.6293 is the critical value of the wavenumber, but 2772.27 arises as the critical value of the 'internal' Rayleigh number, and not of the parameter $\Lambda = GePe^2$. The internal Rayleigh number is defined by Roberts (1967) as the Rayleigh number evaluated for a temperature difference proportional to the uniform rate of heat generation per unit volume, q_0, within the layer,

$$Ra_I = \frac{\beta\, g\, q_0\, L^5}{\nu\, \alpha\, k}. \tag{4.14}$$

We point out that, for the basic state of Couette flow, the effect of viscous dissipation is in fact equivalent to a uniform generation of heat within the fluid, $q_0 = \mu\, u_0^2 / L^2$.

Method	Λ_{cr}	a_{cr}	ω_{cr}
Euler, $\delta z = 10^{-3}$	44302.7698	2.96290196	1016.08305
Euler, $\delta z = 10^{-4}$	44268.9286	2.96282043	1016.76978
Euler, $\delta z = 5 \times 10^{-5}$	44267.0718	2.96281718	1016.80824
Euler, $\delta z = 10^{-5}$	44265.5881	2.96281469	1016.83903
Euler, $\delta z = 5 \times 10^{-6}$	44265.4027	2.96281438	1016.84288
Runge–Kutta (fourth order)	44265.2174	2.96281408	1016.84673
Runge–Kutta (ninth order)	44265.2174	2.96281408	1016.84673

TABLE 1. Large-Pr approximation; critical values of a, Λ and ω for transverse rolls ($\gamma = 0$) with $Pe = 600$; comparison between the Euler method with a fixed step size, δz, the fourth-order Runge–Kutta method with adaptive step-size control and the ninth-order Runge–Kutta method with adaptive step-size control.

The latter relationship can be easily obtained from (2.4), (2.6) and (2.11). Moreover, for longitudinal rolls, the effect of viscous dissipation associated with the velocity disturbances turns out to be negligible. On substituting $q_0 = \mu u_0^2/L^2$ in (4.14), we obtain

$$Ra_I = \frac{\beta g L}{c} \frac{u_0^2 L^2}{\alpha^2} = GePe^2 = \Lambda. \tag{4.15}$$

This justifies the coincidence of the numerical results obtained by Roberts (1967) and those reported in (4.13).

5. Discussion of the results

5.1. *Validation of the numerical method*

A validation of the numerical procedure based on the Runge–Kutta method with adaptive step-size control is carried out by comparison with the Euler method. The latter method is implemented in the Mathematica 7.0 environment through the built-in function `NDSolve`, with the assignment `Method` → "`ExplicitEuler`" and a fixed step-size setting. Decreasing values of the step size, δz, are prescribed as $\delta z = 10^{-3}$ to 5×10^{-6}. The computed values of Λ_{cr}, a_{cr} and ω_{cr} are reported in table 1, referring to the case of transverse rolls ($\gamma = 0$) with $Pe = 600$. This table clearly shows that the Euler method leads to results closer and closer to those obtained through the fourth-order Runge–Kutta method as δz decreases. We note that, the agreement for $\delta z = 5 \times 10^{-6}$ is almost perfect within five significant digits. A further validation of the fourth-order Runge–Kutta method with adaptive step-size control is provided in table 1, by comparison with the ninth-order Runge–Kutta method with adaptive step-size control. In this case, the agreement within nine significant digits is perfect, thus showing that the solution is practically not sensitive to the order of the Runge–Kutta method. We mention that the default adaptive step-size control implemented in the function `NDSolve` is a very efficient algorithm that allows a much faster convergence than the fixed step-size mode of the Euler method. As a result of the validation procedure, all the following computations will be performed by the Runge–Kutta method with the default adaptive step-size control and automatic assignment of the optimal order.

5.2. *The effect of the inclination angle*

The numerical solution of (3.24)–(3.26) for different values of γ allows one to establish the effects of the inclination angle with respect to the critical conditions for the onset of

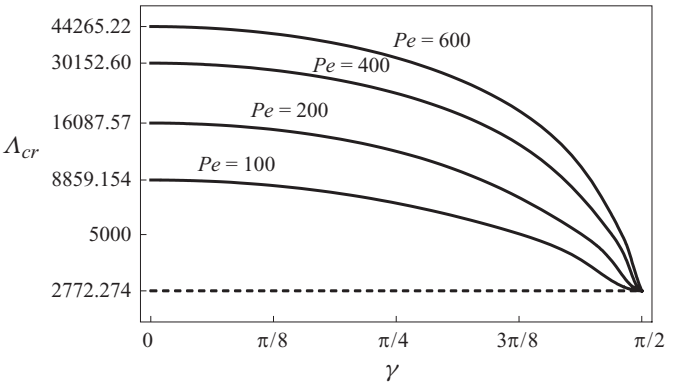

FIGURE 2. Large-Pr approximation; critical value Λ_{cr} versus the inclination angle γ for oblique rolls with different Pe.

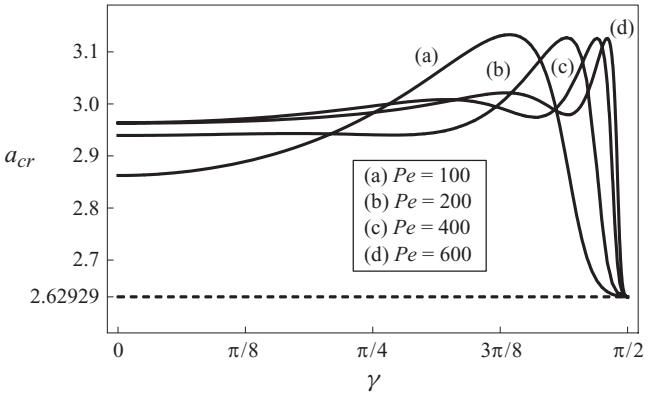

FIGURE 3. Large-Pr approximation; critical value a_{cr} versus the inclination angle γ for oblique rolls with different Pe.

instability. Figure 2 illustrates the dependence of Λ_{cr} on γ for $Pe = 100, 200, 400, 600$. The basic information that can be drawn from this figure is as follows:

(i) for a given Pe, longitudinal rolls ($\gamma = \pi/2$) are the most unstable disturbances, i.e. they correspond to the lowest value of Λ_{cr};

(ii) Λ_{cr} is a monotonic decreasing function of γ;

(iii) the dependence of Λ_{cr} on γ becomes more and more marked as Pe increases.

As will be pointed out in the following section, there exists a narrow range of Pe, close to the limiting case $Pe \to 0$, where the statement (i) does not hold.

Figure 3 reveals that the critical wavenumber a_{cr} is not a monotonic function of the inclination angle γ. For a given Pe, there exists a value of γ, different from both 0 and $\pi/2$, where a_{cr} reaches a maximum. The minimum value of a_{cr}, namely 2.62929 as given by (4.13), is attained in the case of longitudinal rolls ($\gamma = \pi/2$).

Figure 4 shows the monotonic decreasing behaviour of ω_{cr} versus γ. There is a very large gap between the high positive value of ω_{cr} associated with the transverse rolls and the vanishing value of ω_{cr} for longitudinal rolls. This gap is markedly amplified as Pe increases. Figure 4 supports the assumption $\omega_{cr} = 0$ leading to a self-adjoint eigenvalue problem in the limit $\gamma \to \pi/2$ (longitudinal rolls).

Figure 5 displays the marginal stability curves, $\Lambda(a)$, for $Pe = 200$, 400, and either longitudinal rolls or oblique rolls having an inclination angle γ slightly smaller

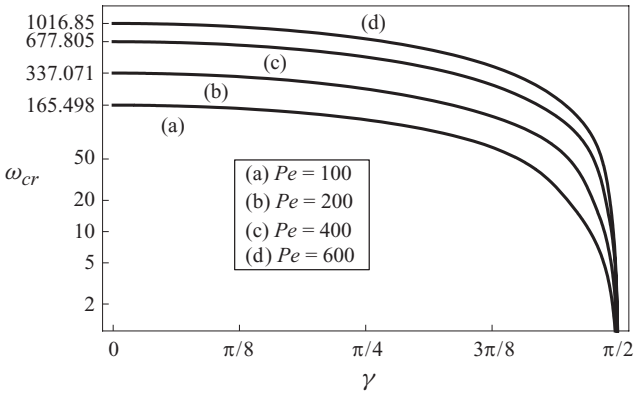

FIGURE 4. Large-Pr approximation; critical value ω_{cr} versus the inclination angle γ for oblique rolls with different Pe.

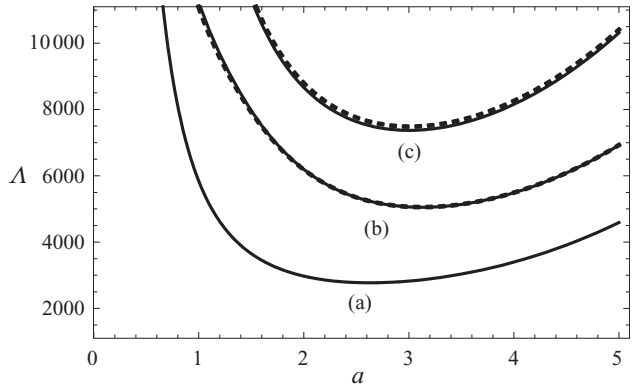

FIGURE 5. Large-Pr approximation; marginal stability curves with: $\gamma = \pi/2$ (line (a)); $\gamma = 7\pi/16$ and $Pe = 200$ (line (b) solid); $\gamma = 15\pi/32$ and $Pe = 400$ (line (b) dashed); $\gamma = 3\pi/8$ and $Pe = 200$ (line (c) solid); $\gamma = 7\pi/16$ and $Pe = 400$ (line (c) dashed).

than $\pi/2$. The most interesting feature of this figure is that the marginal stability curves have the typical shape found for the Rayleigh–Bénard problem (Drazin & Reid 2004). We also note that the marginal stability curves for $Pe = 200$ are almost coincident with those for $Pe = 400$ even though they correspond to different values of γ: $(3\pi/8, 7\pi/16, \pi/2)$ for $Pe = 200$; $(7\pi/16, 15\pi/32, \pi/2)$ for $Pe = 400$. This feature suggests an approximate scale symmetry of the marginal stability condition, that holds in a neighbourhood of $\gamma = \pi/2$. In other words, the function $\Lambda(a)$ is seemingly left invariant when we rescale $Pe \to H\,Pe$ and $(\pi/2 - \gamma) \to (\pi/2 - \gamma)/H$, where H is a real positive constant. This approximate symmetry is conceivable also on the basis of figures 2 and 3.

5.3. *The effect of the Péclet number*

The change of the critical value $(\Lambda_{cr}, a_{cr}, \omega_{cr})$ as Pe increases is represented in figures 6–8, for oblique rolls with $\gamma = \pi/4$ and for transverse rolls $\gamma = 0$. For both kinds of disturbances, Λ_{cr} and ω_{cr} are increasing functions of Pe. On the other hand, as it is shown in figure 7, a_{cr} displays a non-monotonic behaviour as Pe increases.

Figures 6 and 8 suggest that, for large values of Pe, Λ_{cr} and ω_{cr} are approximately a linear function of Pe.

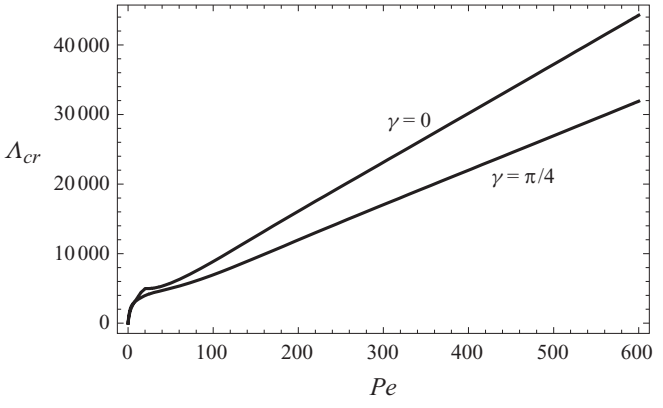

FIGURE 6. Large-Pr approximation; critical value Λ_{cr} versus Pe for oblique rolls with $\gamma = \pi/4$ and $\gamma = 0$ (transverse).

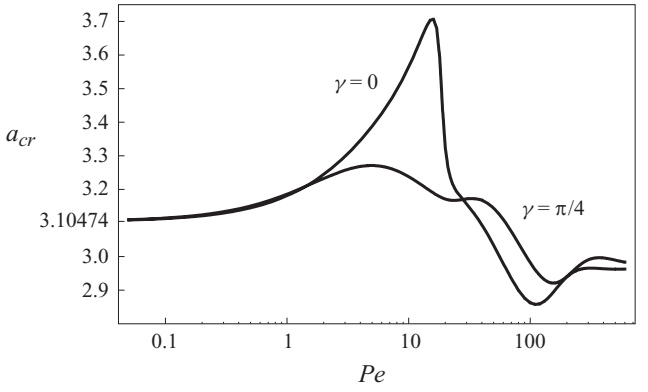

FIGURE 7. Large-Pr approximation; critical value a_{cr} versus Pe for oblique rolls with $\gamma = \pi/4$ and $\gamma = 0$ (transverse).

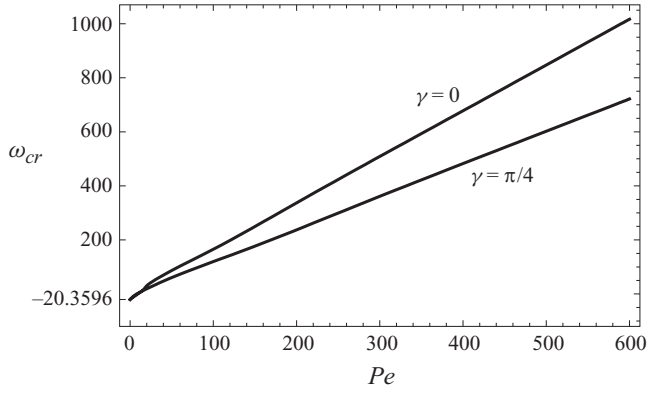

FIGURE 8. Large-Pr approximation; critical value ω_{cr} versus Pe for oblique rolls with $\gamma = \pi/4$ and $\gamma = 0$ (transverse).

One may easily infer that, in the limit $Pe \to 0$, (3.24)–(3.26) can be rewritten as

$$f'''' - 2a^2 f'' + a^4 f - ah = 0, \tag{5.1}$$

$$h'' - (a^2 - \mathrm{i}\omega)h + 2\mathrm{i}\Omega f'' + 2\mathrm{i}a^2\Omega f = 0, \tag{5.2}$$

$$\left.\begin{array}{lll} z=0: f=0, & f'=0, & h'=0, \\ z=1: f=0, & f'=0, & h=0, \end{array}\right\} \tag{5.3}$$

where

$$\Omega = \frac{\Lambda}{Pe}\cos\gamma. \tag{5.4}$$

The critical values of (a, Ω, ω) at the onset of instability may be evaluated by solving the eigenvalue problem (5.1)–(5.3) by means of the numerical procedure described in § 4. Thus, one obtains

$$a_{cr} = 3.10474, \quad \Omega_{cr} = 1199.54, \quad \omega_{cr} = -20.3596. \tag{5.5}$$

This means that, for oblique rolls with $0 \leqslant \gamma < \pi/2$, the limits for $Pe \to 0$ of a_{cr}, Λ_{cr} and ω_{cr} are

$$a_{cr} \to 3.10474, \quad \Lambda_{cr} \to 0, \quad \omega_{cr} \to -20.3596. \tag{5.6}$$

These limits are confirmed by figures 6–8. Therefore, for every γ with $0 \leqslant \gamma < \pi/2$, there exists a range of small values of Pe such that Λ_{cr} for the oblique rolls is smaller than the critical value of Λ for longitudinal rolls, i.e. 2772.27 as given by (4.13). Then, in this range of small Péclet numbers, the longitudinal rolls are less unstable than oblique rolls, in contrast with the usual behaviour described in the preceding section. We mention that the data for very low values of Pe are hardly significant in practice. In fact, Turcotte *et al.* (1974) considered values of the Gebhart number up to 3, but usually Ge is much lower than 1. Then, as a consequence of (3.27), the critical condition $\Lambda_{cr} = 2772.27$ with $Pe = 10$ implies a critical Gebhart number 27.7227 for the Couette flow to become unstable. We reckon that this critical condition is unlikely to be observed in a real flow system. Far more realistic cases are, for instance, those with $Pe > 1000$, since the associated critical Gebhart number would be smaller than 2.77227×10^{-3}. As a consequence, the range of small Péclet numbers, where the longitudinal rolls are less unstable than oblique rolls, appears to be barely significant from a physicist's perspective.

6. A finite Prandtl number

We now consider the case of finite-Pr disturbances, (3.2)–(3.7), having in mind the case of transverse rolls, $\gamma = 0$. In fact, for a finite Prandtl number, the only case such that two-dimensional oblique rolls defined by (3.14) are compatible with (3.2)–(3.7) is $\gamma = 0$. As can be easily checked, the reason is the term $(PeW \sin\gamma)/Pr$ that appears on the left-hand side of (3.4). If one seeks solutions defined by (3.14), (3.4) is satisfied only if $(PeW \sin\gamma)/Pr = 0$. For finite non-vanishing values of Pr and Pe, this equation implies that either $W = 0$ or $\gamma = 0$ (transverse rolls). The first option, $W = 0$, would lead to trivial solutions, so that one may only consider the second option, i.e. transverse rolls.

We recognize that, among the possible oblique rolls, transverse rolls are the less interesting case, as the flow is usually much more unstable to longitudinal rolls. The latter disturbance modes are not allowed in the finite-Pr case. Thus, this section has just the objective of assessing the validity of the large-Pr approximation. By considering two-dimensional transverse rolls defined by (3.14), we compare the results discussed in the preceding sections for the large-Pr regime with those obtained for a finite Prandtl number.

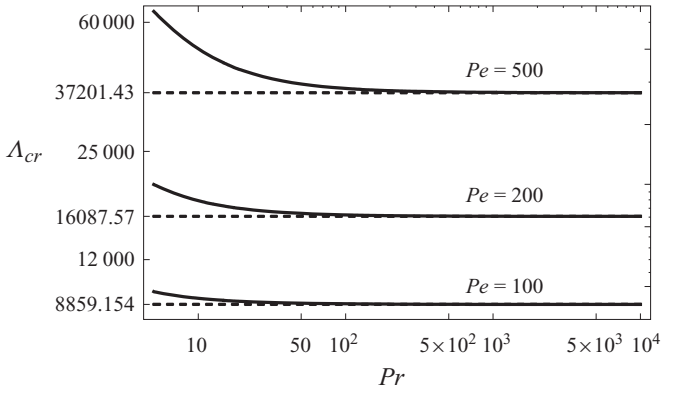

FIGURE 9. Critical value Λ_{cr} versus Pr for transverse ($\gamma = 0$) rolls with $Pe = 100, 200, 500$.

6.1. *Two-dimensional transverse rolls*

Let us assume that $\gamma = 0$ and that (3.14) holds. Then, (3.4) is identically satisfied, while (3.2) is fulfilled by defining a streamfunction $\psi(x, z, t)$ such that (3.19) holds.

As a consequence, one can combine (3.3) and (3.5) in order to encompass the dependence on the pressure disturbance P, so that (3.3), (3.5)–(3.7) and (3.19) yield

$$\left(\frac{\partial}{\partial t} - Pr\nabla^2 + Pez\,\frac{\partial}{\partial x}\right)\nabla^2\psi = -\,Pr\frac{\partial\theta}{\partial x}, \tag{6.1}$$

$$\frac{\partial\theta}{\partial t} + Pez\left(\frac{\partial\theta}{\partial x} + GePe\,\frac{\partial\psi}{\partial x}\right) = \nabla^2\theta + 2GePe\left(\frac{\partial^2\psi}{\partial z^2} - \frac{\partial^2\psi}{\partial x^2}\right), \tag{6.2}$$

$$\left.\begin{aligned} z = 0 : \psi = 0, \quad \frac{\partial\psi}{\partial z} = 0, \quad \frac{\partial\theta}{\partial z} = 0, \\ z = 1 : \psi = 0, \quad \frac{\partial\psi}{\partial z} = 0, \quad \theta = 0. \end{aligned}\right\} \tag{6.3}$$

Plane wave solutions of (6.1)–(6.3) are sought, given by (3.23). In the following, we deal with the marginal stability condition, so that we consider $\lambda = 0$. Then, on substituting (3.23) in (6.1)–(6.3), we obtain

$$f'''' - \left[2a^2 + \mathrm{i}\,\frac{aPez - \omega}{Pr}\right]f'' + a^2\left[a^2 + \mathrm{i}\,\frac{aPez - \omega}{Pr}\right]f - ah = 0, \tag{6.4}$$

$$h'' - [a^2 + \mathrm{i}(aPez - \omega)]h + 2\,\mathrm{i}\,\frac{\Lambda}{Pe}\,f'' + \frac{\Lambda}{Pe}\,a\,(Pez + 2\mathrm{i}a)\,f = 0, \tag{6.5}$$

$$\left.\begin{aligned} z = 0 : f = 0, \quad f' = 0, \quad h' = 0, \\ z = 1 : f = 0, \quad f' = 0, \quad h = 0. \end{aligned}\right\} \tag{6.6}$$

The same numerical solution procedure described in §4 can be applied. We note that here we must give the input values (Pr, Pe, a) and obtain the pair (ω, Λ) as the eigenvalue in the numerical solution of (6.4)–(6.6). Again, the critical values $(\Lambda_{cr}, a_{cr}, \omega_{cr})$, for a given pair (Pr, Pe), are obtained by seeking the minimum of function $\Lambda(a)$, the latter being the eigenvalue Λ that corresponds to the assigned data (Pr, Pe, a).

Figure 9 illustrates the behaviour of Λ_{cr} versus Pr for increasing values of Pe, namely 100, 200 and 500. The critical value Λ_{cr} is a decreasing function of Pr in the

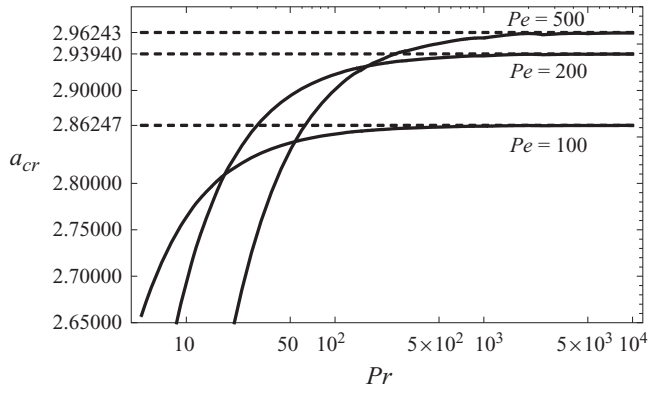

FIGURE 10. Critical value a_{cr} versus Pr for transverse ($\gamma = 0$) rolls with $Pe = 100, 200, 500$.

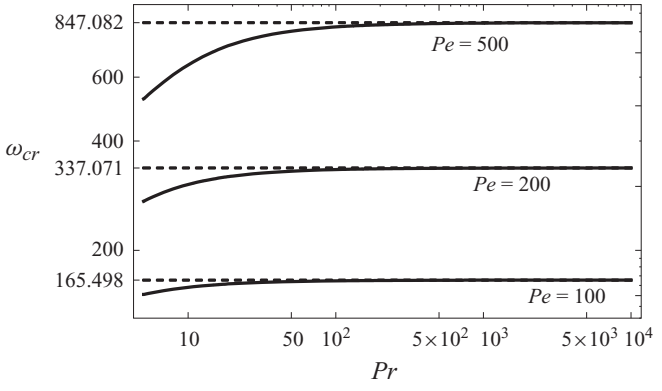

FIGURE 11. Critical value ω_{cr} versus Pr for transverse ($\gamma = 0$) rolls with $Pe = 100, 200, 500$.

ranges considered in figure 9. The results of the large-Pr approximation, analysed in the previous sections, are recovered asymptotically.

Figures 10 and 11 are the companions of figure 9 displaying the behaviour of a_{cr} and ω_{cr}, respectively, for finite values of Pr. Figures 10 and 11 reveal that both a_{cr} and ω_{cr} are increasing functions of Pr for a given value of Pe.

A quantitative comparison between the data reported in figures 9–11 and those obtained in the large-Pr approximation can be established as follows. For a given value of $Pe = 100, 200$ or 500, let us consider the three quantities Λ_{cr}, a_{cr} and ω_{cr} and determine the threshold value Pr_{tr} such that, for $Pr > Pr_{tr}$, each quantity differs from its asymptotic value by less than 5 %. Following this procedure, we see that Pr_{tr} is approximately equal to 9 when $Pe = 100$, 22 when $Pe = 200$ and 61 when $Pe = 500$.

7. Conclusions

A linear stability analysis of the basic Couette flow in a plane channel has been carried out. The viscosity of the fluid has been assumed to be constant, while the density changes have been taken into account through the buoyancy force, thus invoking the Oberbeck–Boussinesq approximation. Boundary conditions have been considered such that the viscous dissipation contribution in the local energy balance is the unique driving mechanism of the convective instability. In particular, an insulated

bottom boundary and a constant temperature top boundary have been considered. A highly viscous fluid with a very large Prandtl number, Pr, has been studied. In the limit $Pr \to \infty$, a complete set of normal modes in the form of two-dimensional oblique rolls has been introduced for modelling the linear disturbances to the basic flow. A numerical solution, based on the Runge–Kutta method, has lead to the determination of the critical conditions for the onset of the convective instability. The main results obtained are the following.

(i) The longitudinal rolls, having the axes parallel to the basic flow direction, are the most unstable modes. The transverse rolls, having the axes perpendicular to the basic flow direction, are the most stable modes. The only exception to this rule is displayed for very small values Pe: a regime where the onset of the instability may occur only for unphysically large values of Ge.

(ii) The governing parameter for the onset of the instability is $\Lambda = Ge\, Pe^2$, where Ge is the Gebhart number and Pe is the Péclet number.

(iii) For longitudinal rolls, the minimum value of Λ at marginal stability, i.e. the critical value Λ_{cr}, is independent of Pe. Its value is $\Lambda_{cr} = 2772.27$.

(iv) A numerical study of the transverse rolls, in the case of a finite Prandtl number, has allowed us to assess the validity of the $Pr \to \infty$ assumption. Numerical tests for $Pe = 100, 200, 500$ revealed that a fair agreement with the large-Pr approximation exists when Pr is greater than 9, 22 and 61, depending on the value of Pe. We mention that, for instance, engine oils usually have values of Pr greater than 100.

REFERENCES

Barletta, A., Celli, M. & Rees, D. A. S. 2009 The onset of convection in a porous layer induced by viscous dissipation: a linear stability analysis. *Intl J. Heat Mass Transfer* **52**, 337–344.

Drazin, P. G. & Reid, W. H. 2004 *Hydrodynamic Stability*, 2nd edn. Cambridge University Press.

Finlayson, B. A. & Scriven, L. E. 1966 The method of weighted residuals – a review. *Appl. Mech. Rev.* **19**, 735–748.

Fujimura, K. & Kelly, R. E. 1988 Stability of unstably stratified shear flow between parallel plates. *Fluid Dyn. Res.* **2**, 281.

Hamabata, H. & Takashima, M. 1983 The effect of rotation on convective instability in a horizontal fluid layer with internal heat generation. *J. Phys. Soc. Japan* **52**, 4145–4151.

Ho, T. C., Denn, M. M. & Anshus, B. E. 1977 Stability of low Reynolds number flow with viscous heating. *Rheol. Acta* **16**, 61–68.

Ingersoll, A. P. 1966 Convective instabilities in plane Couette flow. *Phys. Fluids* **9**, 682–689.

Johns, L. E. & Narayanan, R. 1997 Frictional heating in plane Couette flow. *Proc. R. Soc. Lond.* A **453**, 1653–1670.

Joseph, D. D. 1965 Stability of frictionally-heated flow. *Phys. Fluids* **8**, 2195–2200.

Nield, D. A. & Barletta, A. 2010 Extended Oberbeck–Boussinesq approximation study of convective instabilities in a porous layer with horizontal flow and bottom heating. *Intl J. Heat Mass Transfer* **53**, 577–585.

Nouar, C. & Frigaard, I. 2009 Stability of plane Couette–Poiseuille flow of shear-thinning fluid. *Phys. Fluids* **21**, 064104.

Roberts, P. H. 1967 Convection in horizontal layers with internal heat generation. Theory. *J. Fluid Mech.* **30**, 33–49.

Romanov, V. A. 1973 Stability of plane-parallel Couette flow. *Funct. Anal. Appl.* **7**, 137–146.

Subrahmaniam, N., Johns, L. E. & Narayanan, R. 2002 Stability of frictional heating in plane Couette flow at fixed power input. *Proc. R. Soc. Lond.* A **458**, 2561–2569.

Sukanek, P. C., Goldstein, C. A. & Laurence, R. L. 1973 The stability of plane Couette flow with viscous heating. *J. Fluid Mech.* **57**, 651–670.

Takashima, M. 1991 The stability of natural convection in an inclined fluid layer with internal heat generation. Part II. *J. Phys. Soc. Japan* **60**, 455–465.

Turcotte, D. L., Hsui, A. T., Torrance, K. E. & Schubert, G. 1974 Influence of viscous dissipation on Bénard convection. *J. Fluid Mech.* **64**, 369–374.

Tveitereid, M. & Palm, E. 1976 Convection due to internal heat sources. *J. Fluid Mech.* **76**, 481–499.

Yueh, C. S. & Weng, C. I. 1996 Linear stability analysis of plane Couette flow with viscous heating. *Phys. Fluids* **8**, 1802–1813.